Surface Science 206 (1988) 1–19
North-Holland, Amsterdam

ADSORPTION AND REACTION OF CO_2 ON Ni{110}: X-RAY PHOTOEMISSION, NEAR-EDGE X-RAY ABSORPTION FINE-STRUCTURE AND DIFFUSE LEED STUDIES

G. ILLING, D. HESKETT *, E.W. PLUMMER *, H.-J. FREUND

Lehrstuhl für Physikalische Chemie I, Ruhr-Universität Bochum, D-4630 Bochum,
Fed. Rep. of Germany

J. SOMERS, Th. LINDNER, A.M. BRADSHAW

Fritz-Haber-Institut der Max-Planck-Gesellschaft, Faradayweg 4–6, D-1000 Berlin 33, Germany

U. BUSKOTTE, M. NEUMANN

Fachbereich Physik, Universität Osnabrück, Barbarastrasse 7, D-4500 Osnabrück,
Fed. Rep. of Germany

U. STARKE, K. HEINZ

Institut für Angewandte Physik, Lehrstuhl für Festkörperphysik der Universität Erlangen-Nürnberg,
Erwin-Rommel-Strasse 1, D-8520 Erlangen, Fed. Rep. of Germany

P.L. DE ANDRES **, D. SALDIN and J.B. PENDRY

The Blackett Laboratory, Imperial College, London SW7 2BZ, UK

Received 31 March 1988; accepted for publication 21 July 1988

Using three different techniques – X-ray photoemission (XPS), near-edge X-ray absorption spectroscopy (NEXAFS) and diffuse LEED – we have studied the adsorption and reaction of CO_2 on Ni{110}. In agreement with previous angle-resolved photoemission (ARUPS) and vibrational electron energy loss (EELS) data both a linear, physisorbed molecule and a bent, chemisorbed species $CO_2^{\delta-}$ are found. An evaluation of the XPS line intensities shows that the stoichiometry of the chemisorbed species is 1 to 2 in carbon and oxygen. The polarisation dependence of the NEXAFS indicates that the physisorbed molecule lies with its axis parallel to the surface and that the molecular plane of the $CO_2^{\delta-}$ species is perpendicular to the surface. There is no clear preferential azimuthal orientation. This is in agreement with a diffuse LEED analysis where equal numbers of bent molecules adsorbed on atop sites and oriented along the ⟨100⟩ and ⟨110⟩ directions gave the best fit to the data.

---

* Permanent address: Department of Physics, University of Pennsylvania, Philadelphia, PA 19104, USA.

** Permanent address: Instituto de Materiales, c/Serrano 144, E-28006 Madrid, Spain.

1. Introduction

Adsorption and reaction of CO_2 on transition metal surfaces has received increased interest in recent years [1–11]. ARUPS and vibrational EELS studies on the system Ni{110}–CO_2 [8,9] have indicated that at low temperatures two species are present on the surface: a possibly bent chemisorbed $CO_2^{\delta-}$-species [8,9] and a linear, physisorbed CO_2 molecule. The coordination of the chemisorbed species is not exactly known, but is probably similar to that encountered in inorganic complexes containing CO_2 in the η^2(O) bonding configuration as discussed in ref. [7]. The relative concentration of the physisorbed species can be varied by changing the surface temperature and background CO_2 pressure [8,9]. By 180 K all the physisorbed CO_2 desorbs from the surface at sufficiently low partial pressures; the chemisorbed species remains and can be characterised separately. It does not, however, form an ordered overlayer, thus ruling out a conventional LEED investigation. A thermally activated conversion of the physisorbed molecule into the chemisorbed species appears not to occur. Upon raising the temperature above 190 K, the $CO_2^{\delta-}$ species then dissociates into CO and O, both remaining chemisorbed on the surface. It has therefore been concluded that the bent $CO_2^{\delta-}$ species is an intrinsic precursor for the dissociation of CO_2 and that it could also be an important intermediate in heterogeneous CO oxidation. There are several open questions concerning the nature of the chemisorbed species. For example, it has not yet been proven that the oxygen/carbon stoichiometry is indeed 2 : 1; nor has a detailed study of the orientation and adsorption site been carried out. The first problem can be solved in a straightforward way, namely, via the analysis of the corresponding O and C 1s XPS intensities in comparison with physisorbed CO_2. The second question is more involved; a glance at fig. 1 shows some of the possible structures that could occur. Previous ARUPS and HREELS results [8,9] are compatible with C_{2v} symmetry of the adsorbate complex which suggests two possible coordinations with either the carbon atom (a) or the oxygen atoms (b) down. A comparison with the site adopted by the formate ion on Cu{110}, where the molecular plane of the HCOO-species is aligned in the [110] azimuth and the oxygen atoms are bound to the metal favours the η^2 oxygen coordination [12,13]. This bonding geometry is also favoured by cluster calculations [7] but so far there has been no direct experimental evidence.

SEXAFS is in principle a method that allows structural determination of a disordered molecular adsorbate system [12,14] if the relatively long measuring times required to accumulate spectra with reasonable signal/noise ratio can be tolerated. Unfortunately, in the present case the stability of the adsorbate hampers the accumulation of good SEXAFS data. However, if the photon energy scan is limited to the near edge region (the NEXAFS), the polarisation dependence of the molecular resonances can be used to determine the orienta-

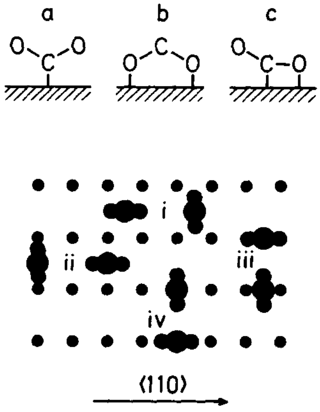

Fig. 1. Top: Possible local adsorption geometries for the chemisorbed $CO_2^{\delta-}$ species on Ni{110}. Bottom: Possible adsorption sites, drawn for the local geometry (b) with the O atoms down. (i) hollow sites, (ii) long bridge sites, (iii) short bridge sites, (iv) on top sites.

tion of the species on the surface [15,16]. This is due to the fact that the absorption intensity from the transition of a core electron into an unfilled molecular orbital is given by

$$I \sim (\boldsymbol{E} \cdot \boldsymbol{M})^2 = (\boldsymbol{E} \cdot \langle \Psi_f | \boldsymbol{M} | \Psi_i \rangle)^2, \tag{1}$$

where $\boldsymbol{M}$ is the electric dipole vector associated with the transition. For example, an isolated diatomic molecule shows polarisation dependences of its σ and π resonances given by

$$I_\sigma \sim (\boldsymbol{E} \cdot \boldsymbol{M}_z)^2 \sim \cos^2\alpha, \quad I_\pi \sim (\boldsymbol{E} \cdot \boldsymbol{M}_{x,y})^2 \sim \sin^2\alpha, \tag{2}$$

where α is the angle between the $\boldsymbol{E}$ vector and the internuclear (z) axis. The main requirements for NEXAFS are that the molecule or molecular fragment retains at least one symmetry element and that there is no ambiguity as to the number and assignment of the resonances [16].

Another technique which can be applied to structural studies of disordered systems is diffuse LEED. Although the adsorption of many molecular systems display no long range order and thus no superstructure spots appear in the diffraction pattern, there may be a considerable background intensity superimposed on the sharp pattern from the well-ordered substrate. As demonstrated in earlier work [17–19], this diffuse background reflects the local adsorption structure. Electrons scattered from different molecules adsorbed on symmetrically equivalent sites (as in a lattice gas arrangement) contribute coherently to the total intensities. Thus the observed diffuse intensities factorise according to

$$I(\boldsymbol{k}_{\parallel}, E) = I_0(\boldsymbol{k}_{\parallel}, E)S(\boldsymbol{k}_{\parallel}), \tag{3}$$

where I_0 is the contribution from a single molecule and S the structure factor appearing as a result of interference between different molecules. Fortunately S is independent of energy for fixed $\boldsymbol{k}_{\parallel}$ and so by construction of the logarithmic derivative with respect to energy

$$L = \frac{\mathrm{d}I/\mathrm{d}E}{I} = \frac{\mathrm{d}I_0/\mathrm{d}E}{I_0}, \tag{4}$$

the unknown structure factor cancels. However, this has to be paid for by an additional measurement (and calculation) of I at another energy.

In the present paper we describe the results of XPS, NEXAFS and DLEED studies on the adsorption system Ni{110}–CO_2 carried out in three laboratories. Whilst our understanding of the quite complex system is still incomplete, we feel that considerable progress has now been made, particularly in the structural characterisation of the chemisorbed species.

2. Experimental

The XPS data were taken in an ultra-high vacuum (UHV) photoelectron spectrometer (Leybold-Heraeus LHS 10) which was equipped with a spatially fixed 100 mm radius hemispherical analyser with pre-retardation, and sample preparation facilities. The Ni{110} crystal was heated resistively and cleaned by sputter–anneal cycles until AES showed no indication of surface contamination. The spectra were excited by Al Kα radiation. The dwell time per data point was between 3 and 30 s, as indicated in fig. 2a. To record a spectrum with reasonable signal/noise ratio took about 5 to 50 min (100 data points per spectrum).

The NEXAFS experiments were performed in a magnetically shielded (UHV) system (VG Scientific, ADES 400) containing facilities for low energy electron diffraction (LEED), Auger spectroscopy (AES), residual gas analysis with a mass spectrometer and electron energy analysis. The electron analyser is rotatable in two orthogonal planes and electrons are collected within an acceptance angle of $\pm 1.5°$. Radiation from the electron storage ring BESSY was used together with the Fritz-Haber-Institut high energy toroidal grating monochromator [20]. In the energy range between 250 and 800 eV the monochromator provides over 10^{12} photons/s · eV at a ring current of ~ 300 mA. The base pressure of the UHV system was 5×10^{-11} mbar. The Ni{110} crystal was spot-welded between two tungsten wires mounted on a sample manipulator. It was oriented such that the incident light was polarised in either the ⟨110⟩ or the ⟨001⟩ azimuth of the Ni{110} surface. The procedures for sample cleaning were identical to those described above.

The NEXAFS spectra were recorded by monitoring the oxygen and carbon Auger yields in an ~ 12 eV wide window centered at 511 and 263 eV, respectively, as a function of photon energy. The Auger electron emission was detected at an angle out of the incident plane so as to minimise direct photoemission features and to allow maximum variation of the incident angle. The latter was varied by rotating the sample relative to the light beam; the Auger emission angle was kept constant by simultaneously moving the electron analyser with the sample. With a dwell time of 0.5 s/data point (120 points for a 60 eV scan) typically five scans were taken to achieve reasonable signal/noise ratios at the O K edge. The NEXAFS spectra presented are difference spectra (with and without adsorbate) and have been normalised to the absorption step height and not, as was done previously [21,22], to the intensity of the metal valence band photoemission signal, which is also present in the spectrum along with the NEXAFS features. The photon energy scale, which at the time of the measurements was unfortunately not calibrated with particular accuracy, has been set such that the leading edge of the $CO_2^{\delta -}$ π resonance coincides with the XPS binding energy relative to E_F (see table 1). There is no real justification for this procedure although it does put the position of the π resonance of physisorbed CO_2 at its gas phase value at the C edge and a few tenths of an eV above it at the O edge.

The diffuse LEED experiments were carried out in a further UHV system also equipped with facilities for Auger and vibrational EELS. In this case the sample heating was realised by electron bombardment. Cleaning procedures were identical to those used in the other experiments. The intensities were recorded using a computer-controlled TV-camera as described in detail elsewhere [23]. In order to avoid any residual gas adsorption the intensity distribution was stored on magnetic tape from which the intensity data were taken off-line. The total measuring time was thus reduced to below 5 min. For the quantitative measurement of intensities the video frame was horizontally scanned with a vertical slit along which the analogue signal was digitised, giving a two-dimensional intensity map. (For details of the measurement procedure, see ref. [24].) In order to get rid of the background caused by the clean crystal, for example from defects or thermal diffuse scattering, the intensity map of the clean crystal was subtracted from that of the adsorbate system.

In all three investigations no extra Bragg features could be seen in LEED on admission of CO_2; only the diffuse scattering described above was observed. The interaction of CO_2 with ion pumps and ion gauge filaments invariably led to problems because of the formation of CO and its preferential adsorption by the sample. Ion pumps and all filaments were therefore switched off during admission of CO_2. In addition, the chambers were flushed repeatedly with CO_2 prior to starting the experiment.

3. Results and discussion

3.1. XPS

Fig. 2 shows the O 1s and C 1s Al Kα spectra from a Ni{110} crystal after exposure to 1.3×10^{-6} mbar · s CO_2 at $T = 150$ K. A constant background has been subtracted. The spectra consist of two well separated peaks with binding energies as given in table 1. The values are in excellent agreement with those measured for Fe(poly)–CO_2 [11]. We assign these two peaks to physisorbed CO_2 and chemisorbed $CO_2^{\delta-}$ as was proposed in our earlier photoemis-

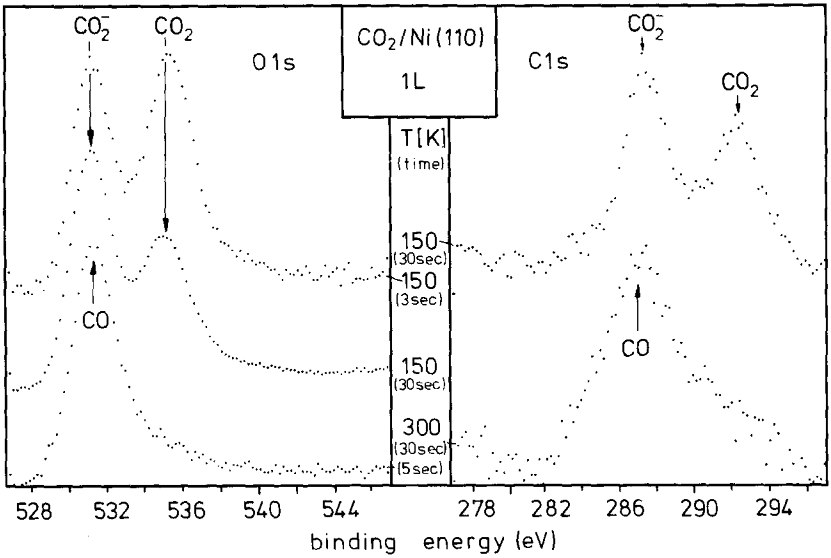

Fig. 2. C 1s and O 1s photoelectron spectra of adsorbed CO_2 after 1 L exposure at 150 and 300 K. The dwell time per data point is indicated. Note the time-dependent X-ray induced transformation of physisorbed CO_2 to $CO_2^{\delta-}$ in the O 1s spectra at $T = 150$ K.

Table 1
Binding energies (relative to E_F) in eV (free molecule binding energies are relative to E_{vac} [25])

		C 1s	O 1s
	CO_2 (gas)	297.5	540.8
Ni(110)	CO_2 (phys)	291.2	534.7
	$CO_2^{\delta-}$	286.4	531.1
	CO	285.6	531.5
Fe(poly)	CO_2 (phys)	291.5	535.0
	$CO_2^{\delta-}$	286.0	531.0
	CO	285.4	531.6

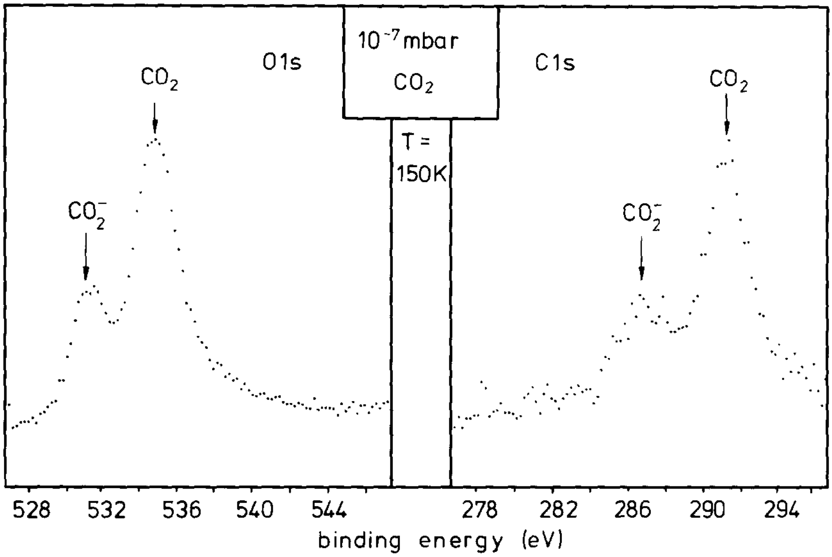

Fig. 3. C1s and O1s photoelectron spectra of CO_2 adsorbed at 150 K and ~10^{-7} mbar CO_2 partial pressure.

sion and EELS measurements [8,9]. The results from the system Fe(poly)–CO_2 have also been interpreted in this way. The observed changes in fig. 3 when the CO_2 pressure in the system increases and CO_2 is condensed on the surface identify the peak at higher binding energy as the one due to physisorbed CO_2.

It should be noted at this point that in order to carry out the intensity analysis and to record spectra in the C1s region with reasonable signal to noise ratio, it was necessary to minimise the exposure to the exciting radiation. The intensity ratio changed upon illumination of the sample from the Al Kα source causing an increase in the intensity of the chemisorbed species at the expense of the physisorbed species (see fig. 2, $T = 150$ K, 3 and 30 s for O1s). The process stops after about 40 min. Since the effect is not observed when the X-ray tube is switched off and since no desorption is observed, we are clearly dealing with a photon-induced (or photoelectron-induced) transformation of one species into the other. A semilog plot of intensity versus time (fig. 4) reveals that the process is first order in physisorbed CO_2 concentration. The mechanism of this transformation is not known at present but its existence obviously hampers the NEXAFS investigation of the physisorbed species. This X-ray-induced transformation must also be taken into account when analysing the relative intensities of the C1s and O1s XPS features. Both sets of spectra have thus been recorded for the same X-ray exposure although this leads to much poorer statistics for the C1s data because of the approximately factor of three difference in the partial photoionisation cross section. Since we know

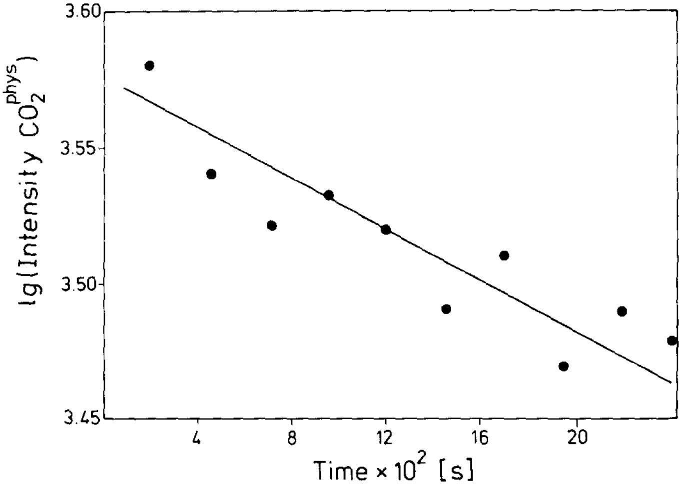

Fig. 4. O1s intensity from the physisorbed CO_2 species at $T = 150$ K as a function of X-ray exposure (time).

that the C1s : O1s intensity ratio from physisorbed CO_2 represents a stoichiometry of C : O = 1 : 2 we can check the stoichiometry of the chemisorbed species. A numerical integration of the peak areas reveals that a ratio of 1 : 2.09, indicating that the stoichiometry of the chemisorbed species is indeed CO_2. The slight deviation from exactly 1 : 2 is most likely due to diffraction effects since the $CO_2^{\delta-}$ and CO_2 are not expected to adsorb in the same configuration on the same site. This stoichiometry determination is in agreement with the findings of Wedler et al. [11] for the system Fe(poly)–CO_2.

3.2. X-ray absorption (NEXAFS)

An X-ray absorption spectrum at the oxygen K-edge for low temperature ($T = 100$ K) and normal incidence ($\theta_E = 90°$) is shown in fig. 5 (top). It consists of two relatively sharp features near threshold and a broad structure spanning the photon energy range 540–552 eV. After raising the temperature to 170–180 K the second peak at the edge disappears while the other features in the spectrum barely change (fig. 6). If the surface is heated to above 200 K a typical CO spectrum with a sharp, intense low energy peak and a very broad, at normal incidence hardly visible, feature at higher photon energy is observed [15]. The carbon NEXAFS spectra reveal the same features as in the corresponding oxygen spectra but with considerably better resolution, as shown in fig. 5 (bottom). However, the count rate is much lower, so that the time necessary to accumulate a spectrum with a reasonable signal-to-noise ratio became very long, considering the low thermal stability of the adsorbate.

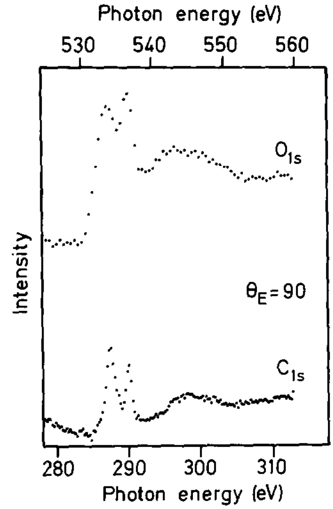

Fig. 5. NEXAFS spectra at the carbon and oxygen edges from the physisorbed CO_2 and the chemisorbed $CO_2^{\delta-}$ species at 100 K.

The second, sharp feature at threshold is clearly due to physisorbed CO_2; a spectrum of the pure species can be obtained indirectly via difference spectra as shown in fig. 6. These are derived by subtraction of the $CO_2^{\delta-}$ spectrum at 170–180 K from the spectrum of the mixed phase at 100 K. Data are shown for both $\theta_E = 90°$ (normal incidence) and $\theta_E = 20°$. In both cases, the difference spectra consist of a single peak, and show within the present signal/noise ratio little indication of a second peak in the range of the broad feature at 540–552 eV. (The subtraction procedure uses the raw data that has

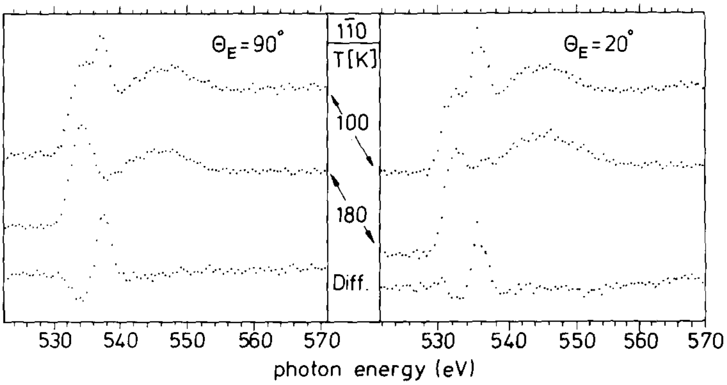

Fig. 6. Difference spectra at the oxygen edge. The spectrum at 180 K has been subtracted from that at 100 K. $\theta_E = 90°$ (left panel), $\theta_E = 20°$ (right panel).

only been normalised to the edge jump height. This results in a small negative peak in the difference spectrum, which can be eliminated by weighting. Even then no significant intensity is present in the region of the broad feature.)

An assignment of the spectral features can be made by consideration of the MO scheme and by comparison with the electron energy loss spectra for free CO_2 [25–29]. The sharp features are clearly due to π-resonances caused by excitation out of O 1s or C 1s into the $2\pi_u$ level of linear CO_2 and the $2b_2$ level of $CO_2^{\delta-}$. The latter is the higher energy component of the two that originate from the splitting of the CO_2 $2\pi_u$ orbital upon bending the molecule. The $6a_1$ component becomes partly occupied upon anion formation, is lowered in energy and can mix with the levels of the metal. The separation between the π-resonances of the two CO_2 species is 2.6 and 2.4 eV at the O edge and C edge, respectively, with the physisorbed CO_2 feature at higher photon energy. These values should be compared with the core electron binding energy differences which are 3.6 and 4.8 eV for O 1s and C 1s ionisation, respectively (see table 1). These larger values can be due to differences in bonding as well as to different screening contributions in the final (ionic) state compared to the NEXAFS experiment. The broad structure at 546 eV photon energy is predominantly due to $CO_2^{\delta-}$ and not to physisorbed CO_2.

As we discuss elsewhere [16], the number and symmetry of the molecular resonances in X-ray absorption spectra may be predicted on the basis of the MO scheme (although it is not necessarily the case that all resonances will actually be observed). In the free CO_2 molecule we predict two σ resonances ($5\sigma_g$ and $4\sigma_u$) at the oxygen edge but only one ($4\sigma_u$) at the carbon edge. Both are observed at the O edge at ~ 7 and ~ 24 eV, respectively, above the π resonance [26]. As expected, the 7 eV feature appears not to be present at the C edge in the electron loss data of Wight and Brion [25]. On the other hand, the spectra at both edges show additional peaks due to multielectron excitations. Since the perturbation of the physisorbed species by the surface is expected to be very small, we would expect its spectrum to be essentially the same as that of the free molecule. It is unclear at present why this is not the case, although the σ-resonances are weak and broad in the Wight and Brion data and could be lost in the noise here (particularly in difference spectra such as those of fig. 6).

How does the putative reduction in symmetry of the chemisorbed species affect this picture? Two σ-type resonances are still expected and may be designated $7a_1$ and $5b_1$, corresponding to the levels $5\sigma_g$ and $4\sigma_u$ of the unperturbed molecule. The selection rules may be simply derived for a species of expected C_{2v} symmetry (see table 2). Both resonances are now allowed at both edges but have different polarisation dependences. The broad feature observed at 540–552 eV probably contains both these resonances, as in the case of the formate species on Cu{110} [12,13]. Fig. 7 shows that the feature is broader for $\theta_E = 20°$ and that its centre of gravity moves to higher photon

Table 2
Symmetry and polarisation of resonances in $CO_2^{\delta -}$ (C_{2v} symmetry; the z axis is in the C_2 axis and the x axis in the molecular plane)

Core	Transition	Polarisation
O1s	$1a_1 \rightarrow 2b_2(\pi)$	y
	$1a_1 \rightarrow 7a_1$	z
	$1a_1 \rightarrow 5b_1$	x
O1s	$1b_1 \rightarrow 2b_2(\pi)$	Forbidden
	$1b_1 \rightarrow 7a_1$	x
	$1b_1 \rightarrow 5b_1$	z
C1s	$2a_1 \rightarrow 2b_2(\pi)$	y
	$2a_1 \rightarrow 7a_1$	z
	$1a_1 \rightarrow 5b_1$	x

energy compared to $\theta_E = 90°$. This may mean that the E_z component is more effective in exciting the $1b_1 \rightarrow 5b_1$ transition than is the E_x component in exciting $1a_1 \rightarrow 5b_1$. In any case, it is not possible to use the σ-type resonances at the oxygen edge for orientation determination for reasons which become clear on examining table 2. At the carbon edge, where it is in principle possible to determine azimuthal alignment if the two resonances can be distinguished, our data is unfortunately not of good enough quality. The C1s spectrum of

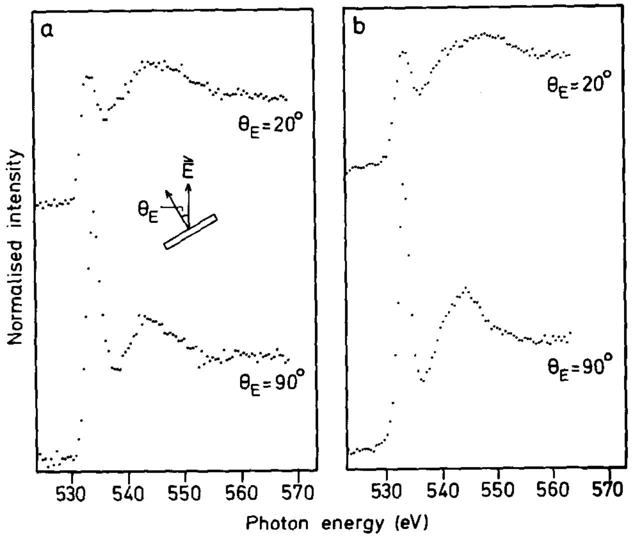

Fig. 7. (a) O NEXAFS spectra from $CO_2^{\delta -}$ at $T = 180$ K taken with the E vector in the ⟨110⟩ azimuth for $\theta_E = 90°$ and 20°. (b) O NEXAFS spectra from $CO_2^{\delta -}$ at $T = 180$ K taken with the E vector in the ⟨100⟩ azimuth for $\theta_E = 90°$ and 20°.

fig. 5 is no exception to this: there is the possibility that CO adsorption from the ambient has occurred here during the 1 h scan time. An alternative assignment of the broad peak should also be considered at this point. The $6a_1$ component of the CO_2 $2\pi_u$ orbital, which is occupied and observable in photoemission [8], can mix with metal levels. The "bonding" combination would be below the Fermi level as observed in photoemission and the "anti-bonding" combination above, possibly shifted past the $2b_2$ component. The symmetry of this state would also be a_1 i.e. the same as that of the first σ-type resonance which is expected. It will, however, be largely of metal character with a low amplitude of the wave function at the site of O 1s photoionisation, giving little overlap and a low transition probability. An assignment of the broad feature to a superposition of the two σ-type resonances appears to be the most likely assignment.

Before we discuss the orientation of $CO_2^{\delta -}$ a short comment concerning the geometry of the physisorbed species is appropriate. From the spectra of fig. 6 it is clear that the intensity of the π resonance does not vary strongly with the angle of incidence. This is to be expected if the molecular axis is oriented parallel to the surface, as proposed in ref. [8], since both E_z and E_y (E_x) components can excite the transition. Were the molecular axis oriented perpendicular to the surface, however, the π-resonance intensity would be strongly attenuated at $\theta_E = 20°$. A lying-down configuration for the physisorbed species is thus inferred; it is also the one expected from the available data for diatomics [30,31].

The polarisation dependence of the π-type resonance can be used to obtain more information on the orientation of the chemisorbed species. Fig. 7a shows the data for the $\boldsymbol{E}$ vector aligned in the $\langle 110 \rangle$ azimuth at $\theta_E = 20°$ and $90°$; fig. 7b shows the spectra at the same two angles but with the $\boldsymbol{E}$ vector aligned in the $\langle 100 \rangle$ azimuth. In each case the two spectra have been taken immediately after each other in order to minimise time-dependent effects which are observed if a full angular series is recorded. We return to this point later. Two observations are important. Firstly, the π-type resonance is strongly attenuated at $\theta_E = 20°$ in both azimuths while the intensity of the σ-type resonance (but not necessarily its form) remains roughly constant. Secondly, the relative change in the intensity of the π resonance in the two azimuths is very similar. The π signal is at a maximum when only E_x and E_y components are present which means that the π resonance is probably polarised parallel to the surface. Since the unoccupied π orbital belongs to b_2, the nodal plane coincides with the molecular plane which is therefore oriented perpendicular to the surface. Since only two spectra can be taken at the extreme angles the accuracy of this determination is not very high. However, a geometry with the molecular plane inclined to the surface is rather unlikely and the data clearly rule out the possibility that the molecular plane is parallel to the surface. Since essentially identical behaviour is observed in both azimuths, it is apparent that

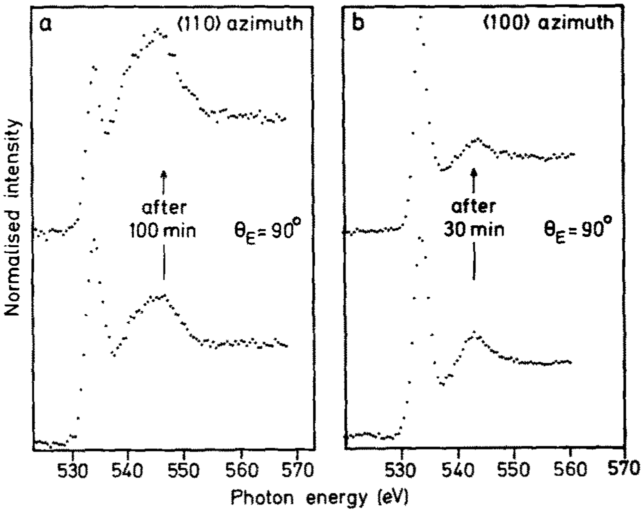

Fig. 8. (a) O NEXAFS spectra from $CO_2^{\delta-}$ at $T = 180$ K taken with the $\boldsymbol{E}$ vector in the ⟨110⟩ azimuth for $\theta_E = 90°$ immediately after adsorption and then 100 min later. (b) O NEXAFS spectra from $CO_2^{\delta-}$ at $T = 180$ K taken with the $\boldsymbol{E}$ vector in the ⟨100⟩ azimuth for $\theta_E = 90°$ immediately after adsorption and then 30 min later.

the molecular plane is not exclusively aligned along ⟨100⟩ or ⟨110⟩. This is contrary to the result found for the formate species on Cu{110} [12,13], where the molecular plane is oriented only in the ⟨110⟩ azimuth. In the $CO_2^{\delta-}$ case we cannot differentiate between two distinct species (one oriented along ⟨110⟩, the other along ⟨100⟩), random alignment or even rotation on one site. The observation of time-dependent effects favours, however, the first alternative: analysis of the full angular series corresponding to fig. 7 soon indicated that time-dependent intensity changes are superimposed on the angular variations. This is illustrated in fig. 8. Repeating the $\theta_E = 90°$ spectrum after 100 min in the ⟨110⟩ azimuth gives rise to a considerable attenuation of the π resonance (fig. 8a). In the ⟨100⟩ azimuth the reverse effect is observed: after 30 min the π resonance has increased in intensity (fig. 8b), albeit in a less spectacular way. We have had unfortunately no opportunity to check these observations systematically since the original data were taken, but they could be symptomatic of a time-dependent re-orientation of the molecular plane from the ⟨100⟩ azimuth in the ⟨110⟩ azimuth.

Finally we note a considerable difference in the observed width of the π resonances at the carbon edge. This is shown in fig. 9 where the region of the π resonance is plotted in more detail. Clearly, the π resonance of the $CO_2^{\delta-}$ species has a larger half width (1.2 eV) than that of physisorbed CO_2 (0.7 eV). This observation could only be made at the carbon edge: at the oxygen edge instrumental broadening due to the monochromator dominates the line width.

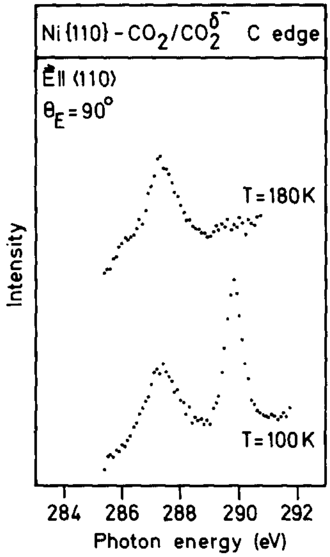

Fig. 9. The π resonance at the carbon edge at 100 K (physisorbed CO_2 and $CO_2^{\delta-}$) and 180 K ($CO_2^{\delta-}$).

There was no evidence for more than one component in the $CO_2^{\delta-}$ π resonance at the carbon edge which otherwise could provide an explanation for the increased width. In fact, one possible interpretation of the measurements described above was that there are at least two types of $CO_2^{\delta-}$ species, one oriented along the ⟨110⟩, the other oriented along the ⟨100⟩ azimuth. These two species would be chemically inequivalent, which might lead to two π resonances rather close in energy. From the width of the observed resonance a separation as high as 0.4 eV would be possible, so that this explanation cannot be ruled out. Also likely, however, is a chemical effect whereby hybridisation of the $2b_2$ level with metal states occurs, leading to line broadening.

3.3. Diffuse LEED

The diffuse intensities were measured at two energies, 70 and 75 eV with respect to the Fermi energy, where the scattered intensity was particularly high. CO_2 was admitted at 130 K crystal temperature. Heating to 190 K produced exclusively the chemisorbed species. Vibrational EELS was used to check this and, at the same time, to ensure that further dissociation had not taken place [9]. In order to minimise multiple scattering between adsorbate molecules the CO_2 coverage was held as low as possible. An exposure of $\sim 10^{-7}$ mbar · s proved to be sufficient to detect the diffuse scattering inten-

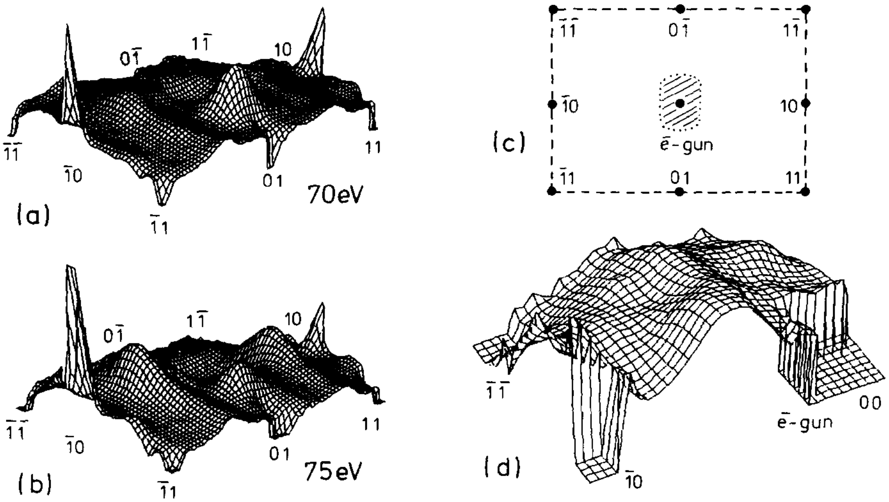

Fig. 10. Diffuse intensities for Ni{110}–CO_2 at $T = 190$ K and energies (a) 70 eV and (b) 75 eV extending over four unit meshes as indicated in (c). The map of the Y-function is displayed in (d) for one unit mesh, whereby the areas corresponding to the electron gun and the Bragg beams have been set to the negative maximum of Y.

sity reliably. Figs. 10a and 10b display the diffuse intensity maps as measured for energies of 70 and 75 eV, respectively. The data corresponding to normal incidence of the primary beam cover the four symmetrically equivalent unit mesh areas as indicated in fig. 10c. The intensities of the Bragg beams were cut away if they had not already been eliminated by the clean subtraction procedure. The two intensity maps clearly differ leading to a non-vanishing logarithmic derivative $L = I'/I$. This is constructed by expanding the higher energy map to the size of the low energy one followed by subtraction and normalisation. The expansion is necessary to take the derivative at constant $\boldsymbol{k}_{\parallel}$ [24]. The result is displayed in fig. 10d. Instead of L the so-called Y-function

$$Y = L/\left(1 + L^2 V_{oi}^2\right), \tag{5}$$

where V_{oi} is the imaginary part of the inner potential ($V_{oi} = 4$ eV [17]), is used in order to avoid divergencies for small values of I. The map in fig. 10d extends only over one unit mesh; an improvement in the data was achieved by averaging over all four systematically equivalent meshes. As there was no coverage measurement facility available, we cannot give absolute figures for the degree of coverage. However, it was definitely far below saturation and in this low coverage regime the resulting Y-function map was independent of coverage.

We employed the Pendry R-factor [32], a statistical correlation factor, to monitor the mean-square deviation between experiment and several theoretical models (see fig. 1). In each case, the height of the C atom and the O–C–O bonding angle were varied systematically; an average over two configurations parallel and perpendicular to the ⟨110⟩ azimuth was taken since it was found that one configuration on its own did not yield a satisfactory fit. For the lowest R-factors, the relative populations of the two configurations were varied and we found a very broad minimum in the R-factor around the case of equal populations. Unlikely appear to be (i) the hollow, (ii) the long bridge and (iii) the short bridge sites with best R-factors of 0.25, 0.20 and 0.30, respectively. Definitely more acceptable are the on-top sites (iv). In this case we considered also random orientations of the molecules. This was found to produce a best value for the R-factor of 0.27.

For the symmetric bend with the O atom up (fig. 1a) the best R-factor was 0.15. The optimum configuration was as follows: the C–Ni bond length in molecules parallel to the ⟨110⟩ azimuth was 2.1 Å; the C–O bond angle to the horizontal in the parallel molecules was 0 °; the C–Ni bond length in molecules perpendicular to the ⟨110⟩ azimuth was 2.0 Å and the C–O bond angle to the horizontal in perpendicular molecules was 12 °. The R-factor maps (fig. 11) are plotted as a function of the bend angles of the molecules parallel to the ⟨110⟩ and ⟨100⟩ directions. In fact, for each combination of angles, we have considered the independent variation of the heights of each of the molecules, and the R-factor values plotted in the figure are the optimum ones obtained from this search. Thus, the R-factor maps must be regarded as plotted on a two-dimensional section of a four-dimensional parameter space. We considered the symmetrical bending of the C–O bonds away from the surface and the variation of the R-factor for this case is shown in fig. 11a.

For the symmetric bend with the oxygen atoms down (fig. 1b) the best value of the R-factor was 0.17. The optimum configuration was as follows: C–Ni bond length in molecules parallel to ⟨110⟩ = 1.9 Å; C–O bond angles to horizontal in parallel molecules = 6 °; C–Ni bond length in molecules perpendicular to ⟨110⟩ = 2.3 Å; C–O bond angles to horizontal in perpendicular molecules = 6 °. The corresponding variation of the R-factor as a function of the symmetrical bond angles is illustrated in fig. 11b.

In the asymmetrically bent species (fig. 1c) one of the C–O bonds is parallel to the surface, the other bent upwards. The positions of the inequivalent bonds were interchanged and averages of the resulting DLEED patterns were taken. The best R-factor turned out to be 0.16. The following optimum configuration was found: C–Ni bond length in molecules parallel to ⟨110⟩ = 2.1 Å; C–O bond angle to horizontal in parallel molecules = 6 °; C–Ni bond length in molecules perpendicular to ⟨110⟩ = 1.9 Å; C–O bond angle to horizontal in perpendicular molecules = 12 °. Fig. 11c shows how the R-factor varies as a function of the asymmetric bond angles of the parallel and perpendicular molecules (x and y axes, respectively).

Realistically, the R-factor analysis can distinguish only between structures whose R-factor deviates by more than 20% from the minimum, i.e. by

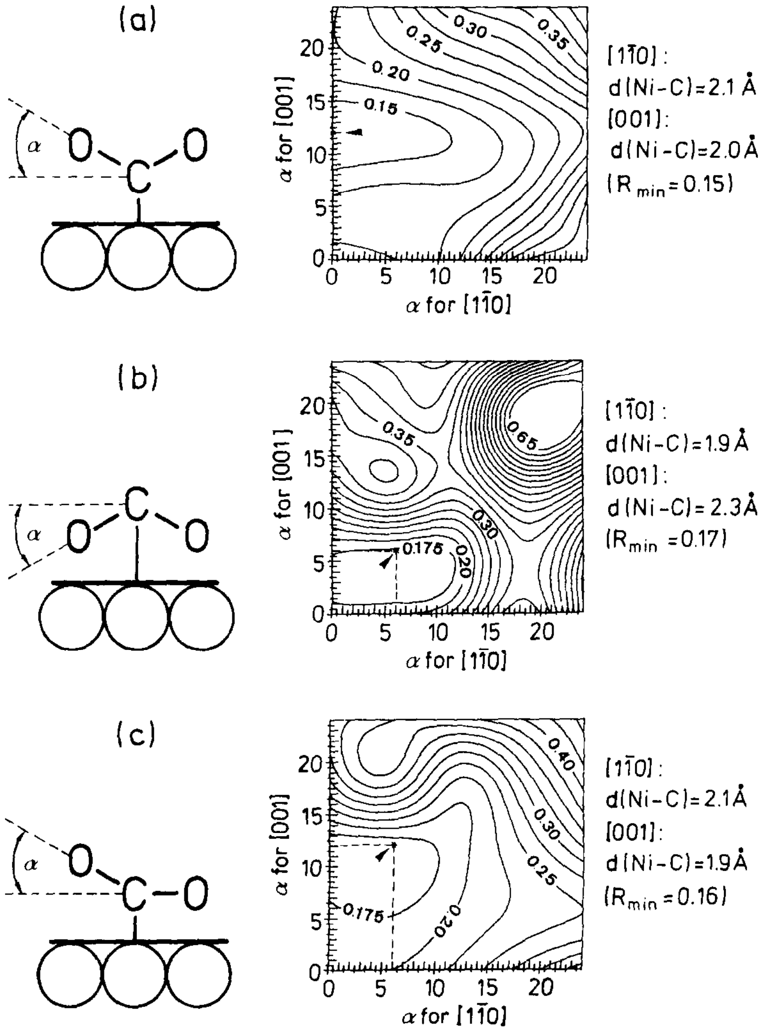

Fig. 11. Variation of the R-factor as a function of bond angle α for molecules oriented parallel to the ⟨110⟩ and ⟨100⟩ azimuths (x- and y-axis, respectively) for (a) symmetrical upward bend, (b) symmetrical downward bend and (c) asymmetrical bend. The Ni–C bond lengths are given in each case for the best fit.

20% × 0.15 = 0.03. Thus, there is a clear indication that the atop sites are occupied rather than the bridge or hollow sites. Nevertheless, more data would be required before it would be possible to distinguish between the three adsorption geometries. The vibrational data [8,9] definitely favour the C_{2v} species (figs. 1a and 1b) and of these, (b) may be the more likely in view of the configuration of the surface formate species [12,13].

4. Summary and conclusions

An analysis of the relative intensities of C 1s and O 1s XPS signals comparing physisorbed and chemisorbed carbon dioxide on Ni{110} shows that the stoichiometry of the chemisorbed species is indeed 1 : 2 in carbon and oxygen. The X-ray beam induces a slow conversion of the physisorbed molecule into the chemisorbed species. The polarisation dependence of the NEXAFS is in agreement with previous ARUPS and EELS measurements [8,9] and indicates that the molecular plane of the bent chemisorbed species is most likely oriented perpendicular to the surface plane but that there is no preferential orientation of the molecular plane along the ⟨110⟩ or ⟨001⟩ surface azimuth. The latter observation is compatible with two different species oriented in each azimuth. In addition, there is a time dependence in the relative intensity of the π resonance that can be interpreted as a preferential re-alignment along ⟨110⟩ under the influence of the X-ray beam. A high resolution experiment at the carbon edge revealed that the width of the π resonance due to physisorbed CO_2 is much smaller than that of the chemisorbed species. Even though two separate peaks could not be resolved, the considerably larger line width of $CO_2^{\delta -}$ may indicate two different species. The broad feature above both O and C edges could not be assigned with confidence but is thought to contain both the $7a_1$ and $5b_1$ resonances. The polarisation dependence of the physisorbed species suggests a lying down configuration. The two time-dependent effects occurring (physisorbed → chemisorbed and re-orientation) together with the very narrow temperature range in which the chemisorbed species can be isolated hinder the full characterisation of this system with NEXAFS. *R*-factor analyses in diffuse LEED studies favour the coexistence of molecules aligned along each principal azimuth. Equal numbers of them on atop sites appears more likely than on hollow, long bridge or short bridge sites. DLEED favours the bent molecule, although the structure determination is not yet final, i.e., the magnitudes and signs of the bond angles could not be reliably determined with the present data set.

Although the chemisorbed species is now somewhat better characterised, the O–C–O angle is still unknown and it is not clear whether the molecule is bent upwards or downwards. By analogy with the surface formate species we might expect the latter, η^2 oxygen coordination geometry to pertain.

Acknowledgement

The authors would like to thank the Deutsche Forschungsgemeinschaft and the Bundesministerium für Forschung und Technologie (BMFT) for financial support.

References

[1] W.H. Weinberg, Surface Sci. 128 (1983) L224.
[2] L.H. Dubois and G. Somorjai, Surface Sci. 128 (1983) L231.
[3] H. Behner, W. Spiess, G. Wedler and D. Borgmann, Surface Sci. 175 (1985) 276.
[4] F. Solymosi and J. Kiss, Surface Sci. 149 (1985) 17.
[5] F. Solymosi and A. Berko, J. Catalysis 101 (1986) 458.
[6] M.P. D'Evelyn, A.V. Hamza, G.E. Godowski and R.J. Madix, Surface Sci. 167 (1986) 451.
[7] H.-J. Freund and R.P. Messmer, Surface Sci. 172 (1986) 1.
[8] B. Bartos, H.-J. Freund, H. Kuhlenbeck, M. Neumann, H. Lindner and K. Müller, Surface Sci. 179 (1987) 59.
[9] H. Lindner, D. Rupprecht, L. Hammer and K. Müller, J. Electron Spectrosc. Related Phenomena 44 (1987) 141.
[10] H.-J. Freund, H. Behner, B. Bartos, G. Wedler, H. Kuhlenbeck and M. Neumann, Surface Sci. 180 (1987) 550.
[11] M. Pirner, R. Bauer, D. Borgmann and G. Wedler, Surface Sci., to be published.
[12] M.D. Crapper, C.E. Riley, D.P. Woodruff, A. Puschmann and J. Haase, Surface Sci. 171 (1986) 1.
[13] D.P. Woodruff, C.F. McConville, A.L.D. Kilcoyne, Th. Lindner, J. Somers, M. Surman, G. Paolucci and A.M. Bradshaw, Surface Sci. 201 (1988) 228.
[14] D. Arvanitis, L. Wenzel and K. Baberschke, Phys. Rev. Letters 59 (1987) 2435.
[15] J. Stöhr and R. Jaeger, Phys. Rev. B 26 (1982) 4111.
[16] A.M. Bradshaw, J. Somers and Th. Lindner, Proc. Solvay Conference on Surface Science (Springer, Berlin) in press.
[17] J.B. Pendry and D.K. Saldin, Surface Sci. 145 (1984) 33.
[18] K. Heinz, D.K. Saldin and J.B. Pendry, Phys. Rev. Letters 55 (1985) 2312.
[19] P.J. Rous, J.B. Pendry, D.K. Saldin, K. Heinz, K. Müller and N. Bickel, Phys. Rev. Letters 57 (1986) 2951.
[20] E. Dietz, W. Braun, A.M. Bradshaw and R.L. Johnson, Nucl. Instr. Methods A 239 (1985) 359.
[21] C.F. McConville, D.P. Woodruff, K.C. Prince, G. Paolucci, V. Cháb, M. Surman and A.M. Bradshaw, Surface Sci. 168 (1986) 221.
[22] J. Somers, Th. Lindner, M. Surman, A.M. Bradshaw, G.P. Williams, C.F. McConville and D.P. Woodruff, Surface Sci. 183 (1987) 576.
[23] K. Heinz and K. Müller, in: Structural Studies of Surfaces, Ed. G. Höhler, Vol. 91 of Springer Tracts in Modern Physics (Springer, Berlin, 1982) p. 1.
[24] K. Heinz, K. Müller, W. Popp and H. Lindner, Surface Sci. 173 (1986) 366.
[25] G.R. Wight and C.E. Brion, J. Electron Spectrosc. Related Phenomena 3 (1974) 191.
[26] D.M. Barrus, R.L. Blake, A.J. Burek, K.C. Chambers and A.L. Pregenzer, Phys. Rev. A 20 (1979) 1045.
[27] F.A. Grimm, T.A. Carlson, W.B. Dress, P. Agron, J.O. Thomson and J.W. Davenport, J. Chem. Phys. 72 (1980) 3041.
[28] F.A. Grimm, Chem. Phys. 53 (1980) 51.
[29] W.R. Daasch, E.R. Davidson and A.U. Hazi, J. Chem. Phys. 76 (1982) 6031.
[30] R.D. Diehl, M.F. Toney and S.C. Fain, Phys. Rev. Letters 48 (1982) 177.
[31] K.C. Prince, G. Paolucci and A.M. Bradshaw, Surface Sci. 175 (1986) 101.
[32] J.B. Pendry, J. Phys. C 13 (1980) 937.